Instantaneous space trajectories of a vector controlled active filter

Jesús Linares-Flores
Benemérita Universidad Autónoma de Puebla, Facultad de Ciencias de la Electrónica
Av. Sn. Claudio y 18 Sur Ciudad Universitaria, Puebla, México.
Tel. 01 (2222) 29 55 00 ext 7400
e-mail: jlinares@ece.buap.mx

Abstract: This paper discusses the transient behavior of a strictly current vector controlled three-phase power active filter, which does not require hysteresis current controllers. Its transient performance is analyzed in terms of its voltage, current and current error instantaneous space trajectories. The vector control strategy determines precisely the region to which a previously defined instantaneous space vector current error belongs. Afterwards, the required inverter output voltage vector that makes this current deviation equal to zero is also determined by the vector controller. Under the knowledge of these vector regions, a set of inverter switching commutation tables are created to produce the best switching action. The vector nature of this control, is analyzed with reference to a selected number of instantaneous space trajectories and time oscillograms of its main vector variables, which are included in the paper.

Keywords: Active filters, current vector control, voltage, current and current error instantaneous space trajectories, three-phase AC/DC converters.

I. INTRODUCTION

The ever increasing use of non-linear loads, as those fed by three-phase AC/DC power converters, has provoked that voltage and current waveforms in the electrical distribution systems are not more sinusoidal. Power active filters have been developed to eliminate harmonic currents and to compensate reactive power in those electrical distribution systems [1-4]. As main compensator unit, the DC/AC three-phase inverter has become the most suitable device [1-10], whose rapid commutation solid state switches allow the right amount of counter harmonic compensating current to be injected to the common coupling point between the non-linear load, and the AC source [3-5, 9]. These counterharmonic compensating currents are characterized by a high harmonic content and very rapid transients [4, 5, 9, 10]. Therefore, the current control has to assure, that the reference current is closely followed by the actual inverter output compensating current [6, 7, 9]. The results presented in this paper show that the described vector control strategy fully complies with this requirement.

The main research objective of this work is to analyze the performance of a vector current controlled active filter, by closely following the behavior of its voltage and current vector space trajectories. The details of the mathematical model and the theoretical fundamentals of this vector-based controlled active filter, that operates at constant switching frequency, without using hysteresis current controllers in each one of the inverter current compensating branches, has been presented in the reference [11].

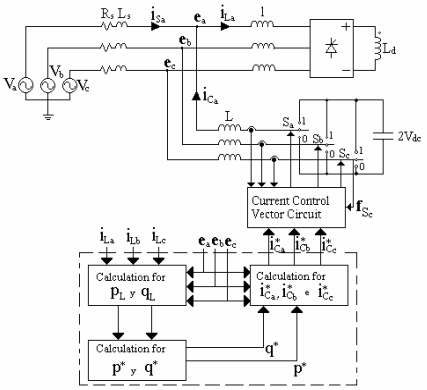

Fig. 1. Current vector controlled active filter.

Fig. 1 shows the power and control blocks of the active filter that instantaneously compensates both, the harmonic currents, and the reactive power. The CD/CA inverter injects the required compensating counterharmonic currents to the common coupling point between the source and the AC/DC harmonics generating load. Three computation blocks are used to determine the reference compensation instantaneous active and reactive powers, and the reference phase currents, from the load phase currents, voltages, and powers. See reference [3].

II. CURRENT VECTOR CONTROL STRATEGY

In Fig. 1, The inverter model is represented in a simplified manner by interrupters $\mathbf{S_a}$, $\mathbf{S_b}$ and $\mathbf{S_c}$ that produces 8 switching modes of the inverter switches, leading to 8 output-vector voltages **V(k)**, as in fig. 2 [11]. The vector differential

equations for each one of the currents compensating branches are:

$$L\frac{di_{Ca}}{dt} = -e_a + VS_a \quad (1)$$

$$L\frac{di_{Cb}}{dt} = -e_b + VS_b \quad (2)$$

$$L\frac{di_{Cc}}{dt} = -e_c + VS_c \quad (3)$$

Where, $VS_{a,b,c} = S_{a,b,c}(k).2V_{dc}$, for a DC/AC inverter with a DC source of $2V_{dc}$[11]. The values for the 8 **V(k)** possibilities produce the inverter output voltage vectors **V(0)** to **V(7)** in fig. 2

In terms of instantaneous space vectors, equations (1) to (3) become (4), with i_C given by (5):

$$L\frac{di_C}{dt} = -e + V(k) \quad (4)$$

$$i_C = \begin{bmatrix} i_{Cd} \\ i_{Cq} \end{bmatrix} = \sqrt{2/3}\begin{bmatrix} 1 & -1/2 & -1/2 \\ 0 & \sqrt{3}/2 & -\sqrt{3}/2 \end{bmatrix}\begin{bmatrix} i_{Ca} \\ i_{Cb} \\ i_{Cc} \end{bmatrix} \quad (5)$$

In (4) and (5), i_C is the compensating current vector, **e** is the voltage vector in the common coupling point of fig.1, and **V(k)** is the inverter voltage vector for each state of commutation. The voltage vector **e**, and the inverter voltage vector **V(k)** are given by (6) and (7). Where $e_{a,b,c}$ and $VS_{a,b,c}$ are the instantaneous values in each phase of the common coupling point and the instantaneous inverter space vectors for the 8 switching possibilities.

$$e = \begin{bmatrix} e_d \\ e_q \end{bmatrix} = \sqrt{2/3}\begin{bmatrix} 1 & -1/2 & -1/2 \\ 0 & \sqrt{3}/2 & -\sqrt{3}/2 \end{bmatrix}\begin{bmatrix} e_a \\ e_b \\ e_c \end{bmatrix} \quad (6)$$

$$V(k) = \begin{bmatrix} V_d \\ V_q \end{bmatrix} = \sqrt{2/3}\begin{bmatrix} 1 & -1/2 & -1/2 \\ 0 & \sqrt{3}/2 & -\sqrt{3}/2 \end{bmatrix}\begin{bmatrix} VS_a \\ VS_b \\ VS_c \end{bmatrix} \quad (7)$$

The compensating error current vector Δi_C, in terms of the reference compensating current vector i_C^*, is given by (8). The substitution of (8) in (4), gives the vector differential (9). Finally, expressing the quantities in the parenthesis of the right hand side of (9), as e_0 in (10), (11) is obtained.

$$\Delta i_C = i_C^* - i_C \quad (8)$$

$$L\frac{d\Delta i_C}{dt} = \left(L\frac{di_C^*}{dt} + e\right) - V(k) \quad (9)$$

$$e_0 = L\frac{di_C^*}{dt} + e \quad (10)$$

$$L\frac{d\Delta i_C}{dt} = e_0 - V(k) \quad (11)$$

In (11), the voltage deviation between e_0 and **V(k)** produces the variation of Δi_C with respect to time. This means that $d\Delta i_C/dt$ is determined by the choice of **V(k)**, since e_0 is the variable that injects the right amount of i_C^* to the common coupling point, (10). Thus, $d\Delta i_C/dt$ determines the current compensation speed in the steady and transient states.

III. SELECTION OF THE INVERTER COMMUTATION MODE

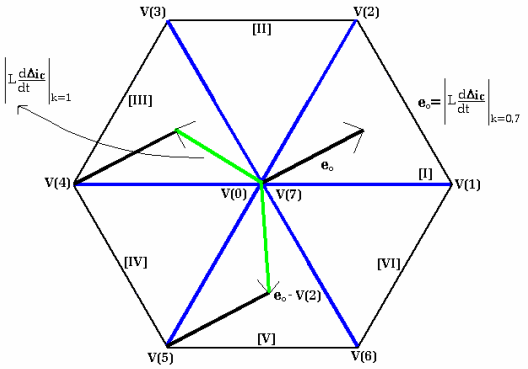

Fig. 2. Vectors **V(k)**, e_0 and $|d\Delta i_C/dt|_{k=0,1,2,7}$.

As shown in fig.2, the inverter can only have a unique output voltage vector **V(k)** from the eight vector possibilities, which has to approach to the required e_0 as much as possible. The method to select **V(k)** can be explained with respect to figs. 2, 3, 4 and 5. Suppose that e_0 is found in the region between **V(1)** and **V(2)**, then, **k=0,1,2** and **7** can be chosen as the inverter switching positions. This gives $|Ld\Delta i_C/dt|_{k=0,\ 1,\ 2,\ 7,}$ which are the three vectors found in the regions **[III]**, **[V]** and **[I]** of fig. 2. These three vectors for **k=1,2** and for **k=0,7** eliminate the compensating current error Δi_C. Fig. 3 shows the derivatives of the current errors for all **k**'s.

It should be clear from fig. 3, that in order to suppress the harmonic current in the steady state, it is necessary to choose

a mode of commutation for the smallest value of the given $\mathbf{d\Delta i_C/dt}$. Therefore, the commutation mode to be chosen is limited to the vertices of the triangle enclosing the vector $\mathbf{e_0}$. That is, if $\mathbf{e_0}$ is detected in region **[I]**, then the commutation mode that is chosen at the inverter output, can be any of these four possibilities **k=0,1,2,7**. The vector that should be chosen depends in the exact position of the compensating vector error $\Delta\mathbf{i_C}$.

Also, in the same fig. 3, $\left|\mathbf{d\Delta i_C/dt}\right|_{\mathbf{k=5}}$, is the greatest opposite direction component to the compensating current vector error $\Delta\mathbf{i_C}$, which can be chosen to achieve quick current response in transient state; while $\left|\mathbf{d\Delta i_C/dt}\right|_{\mathbf{k=0,7}}$ is the smallest component of opposite direction, which is chosen to eliminate harmonic current in steady state. This is the proposed principle of current control strategy.

In the previous explanation however, an assumption was made to define the regions to which $\mathbf{e_0}$ and $\Delta\mathbf{i_C}$ belong. That is, these regions were only assumed. In the following text, these regions will be obtained, departing from the instantaneous values of $\Delta\mathbf{i_C}$.

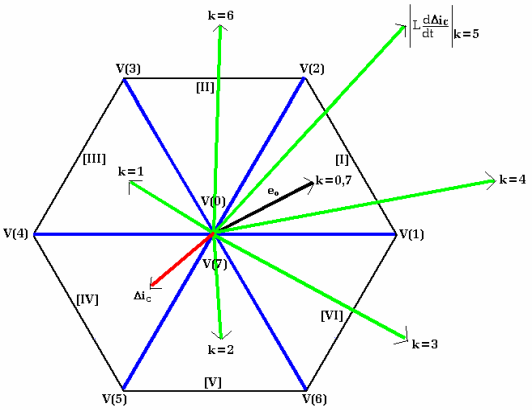

Fig. 3. Derivatives of current errors $\left|\mathbf{L}\,\mathbf{d\Delta i_C/dt}\right|_{\mathbf{k}}$.

IV. DETECTION OF THE REGION TO WHICH THE CURRENT ERROR $\Delta\mathbf{i_C}$ BELONGS.

Fig. 4 and table I show the region to which $\Delta\mathbf{i_C}$ belongs to. Each one of the phase compensating current errors, $\Delta\mathbf{i_{Ca}}$, $\Delta\mathbf{i_{Cb}}$ and $\Delta\mathbf{i_{Cc}}$ are located in the **abc** coordinate system. According to the sign of each phase compensating current errors, the resultant compensating current error vector can be precisely detected in one and only one of the 6 current error regions, 1, 2, ... , 6. For instance for the shown $\Delta\mathbf{i_{Ca}}$, $\Delta\mathbf{i_{Cb}}$ and $\Delta\mathbf{i_{Cc}}$ in fig. 4, $\Delta\mathbf{i_C}$ is located in region 1. Table I shows the corresponding regions of $\Delta\mathbf{i_C}$ according to the signs of $\Delta\mathbf{i_{Ca}}$, $\Delta\mathbf{i_{Cb}}$ and $\Delta\mathbf{i_{Cc}}$.

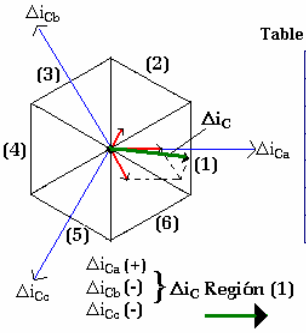

Table I. Determination to which $\Delta\mathbf{i_C}$ belongs

Δi_{Ca}	Δi_{Cb}	Δi_{Cc}	$\Delta\mathbf{i_C}$
+	-	-	(1)
+	+	-	(2)
-	+	-	(3)
-	+	+	(4)
-	-	+	(5)
+	-	+	(6)

Fig. 4. Region to which $\Delta\mathbf{i_C}$ belongs.

V. DETECTION OF THE REGION TO WHICH THE VOLTAGE VECTOR $\mathbf{e_0}$ BELONGS.

Once the region of $\Delta\mathbf{i_C}$ has been detected, it is required to express each phase current deviation by the new **xyz** coordinates, that are rotated 30° counterclockwise, with respect to the reference **abc** coordinates, in order to translate them from the current error vector hexagon to the voltage vector hexagon. Afterwards, the derivative has to be applied to each one of the new transformed $\Delta\mathbf{i_{Cx}}$, $\Delta\mathbf{i_{Cy}}$, and $\Delta\mathbf{i_{Cz}}$ respectively to produce the voltage vectors $\mathbf{L}\,\mathbf{d\Delta i_{Cx}/dt}$, $\mathbf{L}\,\mathbf{d\Delta i_{Cy}/dt}$ and $\mathbf{L}\,\mathbf{d\Delta i_{Cz}/dt}$, which are designed by $\Delta\mathbf{i'_{Cx}}$, $\Delta\mathbf{i'_{Cy}}$, and $\Delta\mathbf{i'_{Cz}}$ in fig. 5. The **abc** to **xyz** transformation and the current error vector derivatives, leading to $\mathbf{e_0}$ determination are shown in fig. 5. Relations (12) to (15) exist between the two coordinate systems and between the current error vectors and their derivatives.

$$\begin{bmatrix} ?\mathbf{i_{Cx}} \\ ?\mathbf{i_{Cy}} \\ ?\mathbf{i_{Cz}} \end{bmatrix} = \frac{\mathbf{1}}{\sqrt{\mathbf{3}}} \begin{bmatrix} \mathbf{1} & \mathbf{0} & \mathbf{-1} \\ \mathbf{-1} & \mathbf{1} & \mathbf{0} \\ \mathbf{0} & \mathbf{-1} & \mathbf{1} \end{bmatrix} \begin{bmatrix} ?\mathbf{i_{Ca}} \\ ?\mathbf{i_{Cb}} \\ ?\mathbf{i_{Cc}} \end{bmatrix} \qquad (12)$$

$$\Delta\mathbf{i_{Cx}} + \Delta\mathbf{i_{Cy}} + \Delta\mathbf{i_{Cz}} = \Delta\mathbf{i_{Cx,y,z}} \qquad (13)$$

$$\mathbf{d}[\Delta\mathbf{i_{Cx}} + \Delta\mathbf{i_{Cy}} + \Delta\mathbf{i_{Cz}}]/\mathbf{dt} = \mathbf{d}\Delta\mathbf{i_{Cx,y,z}}/\mathbf{dt} = \Delta\mathbf{i'_{Cx,y,z}} \qquad (14)$$

$$\mathbf{e_0} = \mathbf{L}\frac{\mathbf{d?\,i_{Cxyz}}}{\mathbf{dt}} + \mathbf{V(k)} \qquad (15)$$

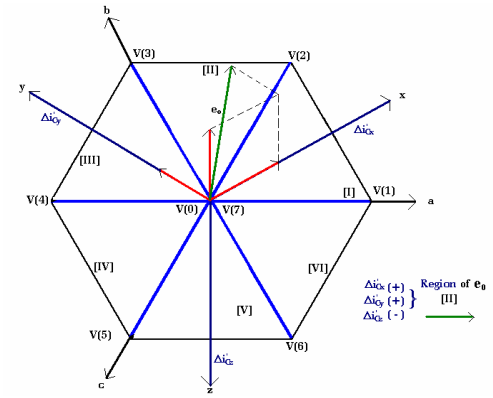

Fig. 5. Region to which $\mathbf{e_0}$ belongs.

As an example of determining the region to which $\mathbf{e_0}$ belongs, consider the cases when the present value of **k** is **0** or **7.** When **k = 0,7**, vector $\mathbf{e_0}$ and vector $\mathbf{L}\mathbf{d}\mathbf{D}\mathbf{i}_{Cx,y,z}/\mathbf{dt}$ are equal, since **V(k)=0**, see (11). Then, the region of $\mathbf{e_0}$ is singularly detected by the sign (plus or minus) of the current deviation derivatives on the **xyz** axes, in this case the region to which $\mathbf{e_0}$ belongs to, is region **[II]**. Table II shows the region of $\mathbf{e_0}$ in terms of the sign of $\mathbf{D}\mathbf{i}'_C$ in **xyz** coordinates. Note that the present position of **V(k)** is also required to determine the $\mathbf{e_0}$ region in the vector voltages hexagon of fig. 5.

Once the regions of $\mathbf{D}\mathbf{i}_C$ and $\mathbf{e_0}$ have been detected**,** the commutation mode of the DC/AC inverter switches are selected according to **Table III**, which summarizes the relations between the region of $\mathbf{e_0}$, the region of $\mathbf{D}\mathbf{i}_C$ and the chosen voltage vector **V(k)**. In **Table III**; **[I]** to **[VI]** are the regions of the vector $\mathbf{e_0}$, and **(1)** to **(6)** are the regions of the vector $\mathbf{D}\mathbf{i}_C$, as shown in figs. 4 and 5 above.

Table II. Region of e_o in terms of the sign of Δi_c in xyz coordinates.

V(k)	$\Delta i'_{Cx}$	$\Delta i'_{Cy}$	$\Delta i'_{Cz}$	e_o
0,7	+	-	-	[I]
	+	+	-	[II]
	-	+	-	[III]
	-	+	+	[IV]
	-	-	+	[V]
	+	-	+	[VI]
1			+	[VI]
			-	[I]
2		-		[I]
		+		[II]
3	+			[II]
	-			[III]
4			-	[III]
			+	[IV]
5		+		[IV]
		-		[V]
6	-			[V]
	+			[VI]

Table III. Region of Δi_c, e_o, and commutation mode V(k)

Region of Δi_c / Region of e_o	1	2	3	4	5	6
I	V(1)	V(2)	V(2)	V(0),V(7)	V(0),V(l)	V(1)
II	V(2)	V(2)	V(3)	V(3)	V(0),V(7)	V(0),V(7)
III	V(0),V(7)	V(3)	V(3)	V(4)	V(4)	V(0),V(7)
IV	V(0),V(7)	V(0),V(7)	V(4)	V(4)	V(5)	V(5)
V	V(6)	V(0),V(7)	V(0),V(7)	V(5)	V(5)	V(6)
VI	V(1)	V(1)	V(0),V(7)	V(0),V(7)	V(6)	V(6)

VI. CURRENT VECTOR CONTROL

Fig. 7 shows the current vector control. The region to which $\mathbf{D}\mathbf{i}_C$ belongs is determined by table I. The sign of each phase deviation current derivative and the present commutation mode of **V(k)** are the entries to table II, which determines the region to which the voltage vector $\mathbf{e_0}$ belongs. The output signals of table I and II, and the present **V(k)** output of table III are the inputs of table III, which is chosen to produce the commutation mode that gives a low harmonic current content during steady state.

Now, during transient state, when $\mathbf{D}\mathbf{i}_C$ gets to be much greater, it is necessary to connect the quick response current control system. To do so it is necessary to choose the commutation mode in which $\mathbf{d}\mathbf{D}\mathbf{i}_C/\mathbf{dt}$ has the greater opposite direction component to $\mathbf{D}\mathbf{i}_C$, as mentioned in section III. The mode is uniquely determined from the region of $\mathbf{D}\mathbf{i}_C$, as shown in table IV. In fig. 6, two hexagons of $\mathbf{D}\mathbf{i}_C$ are presented. The term d expresses the size of the compensating vector error $\mathbf{D}\mathbf{i}_C$, which is the width of the internal hexagon. A relationship exists between the two hexagons, that is $\mathbf{h}=d+a_1$, where a_1 is a very small amplitude margin. If $\mathbf{D}\mathbf{i}_C$ overflows the amplitude **h** of the current hexagon, then the current control system changes from the harmonic current suppression control table III to the quick response current control table IV.

Table IV. Δi_C and V(k) for quick current response

Region of Δi_C	V(k)
1	1
2	2
3	3
4	4
5	5
6	6

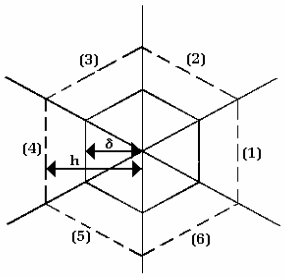

Fig. 6. Commutation hexagon of two states.

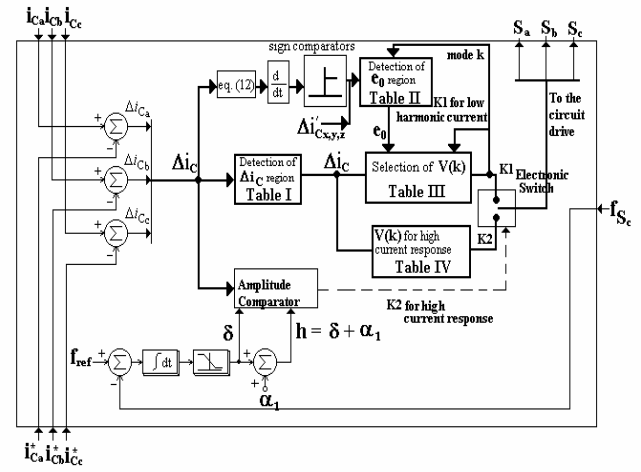

Fig. 7. Current vector control.

VII. SIMULATION RESULTS

The current and voltage time oscillograms of figs. 8, 10 and 12, and the space current trajectories of fig. 9,11 and 13, show the steady and transient states performance of the vector controlled active filter. The steady state occurs during a constant harmonic content in the three-phase AC/DC harmonics generating load, while the transient response occurs when the three-phase AC/DC harmonics generating load varies its firing angle from 30º to 0º. All variables are refered to the power circuit of fig. 1, and to the control circuit of fig. 7.

Fig. 8 shows the instantaneous output phase voltages, and compensating currents being injected by the active filter to the common coupling point of fig. 1, while the space voltage trajectories of **V(k)**, $\mathbf{e_0}$, $\mathbf{Ldi_c/dt}$, and $\mathbf{LdDi_C/dt}$ are shown in Fig. 9. The trajectory of **V(k)** shows the movement of the AC/DC inverter commutation modes, from one voltage vector position to another, to cope with the requirements of the $\mathbf{Di_C}$ variation with time.

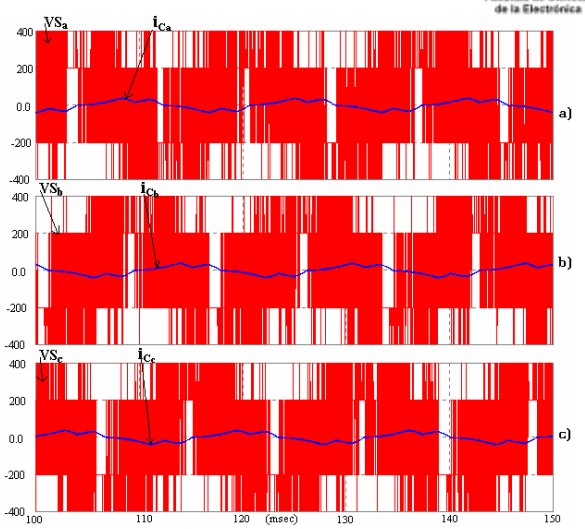

Fig. 8. Instantaneous phase output vector voltages $\mathbf{VS_{abc}}$, and vector compensating currents, $\mathbf{i_{Cabc}}$.

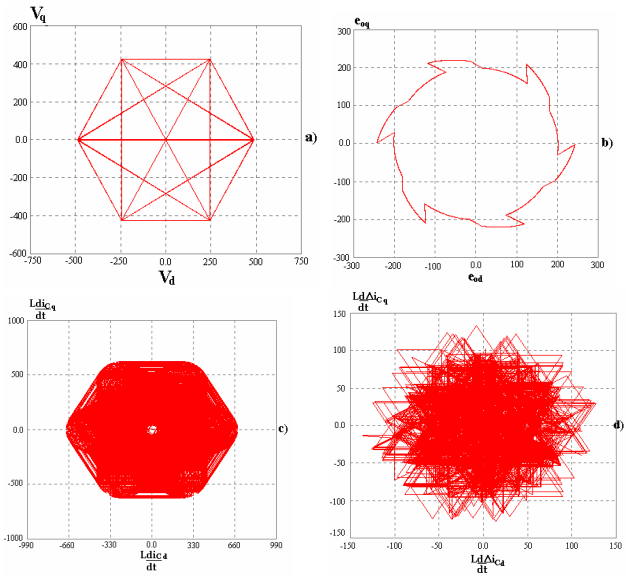

Fig. 9. Steady state space voltage trajectories, a) **V(k)** b) $\mathbf{e_0}$ c) $\mathbf{Ldi_c/dt}$ d) $\mathbf{LdDi_C/dt}$.

The trajectory of $\mathbf{e_0}$ shows the voltage drops due to the derivative of the reference compensation current with time.

Fig. 10 shows the transition between the off and on switching positions of the active filter and its effect in the current error $\mathbf{Di_{Ca}}$. When the active filter is disconnected, no compensating current is fed to the common coupling point of fig.1, and the current error is equal to the reference compensating current. Once the filter is connected, it injects the right amount of compensating current to the common coupling point bringing the current error to a value close to zero. The difference

between $\mathbf{i}^{*}_{\mathbf{Ca}}$ and $\mathbf{i}_{\mathbf{Ca}}$ can be barely seen in the darkest portion of the oscillogram of fig. 10a.

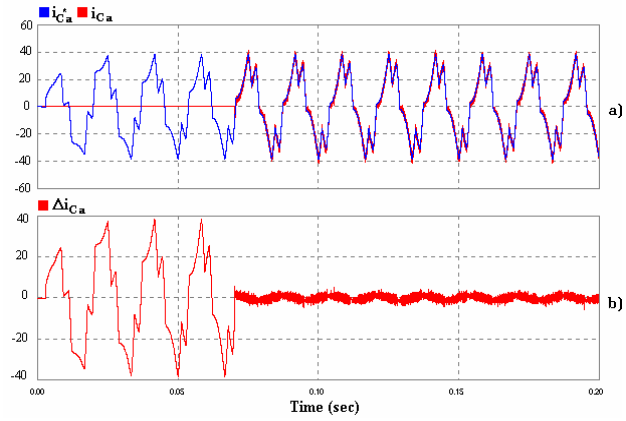

Fig. 10. a) Compensation currents $\mathbf{i}^{*}_{\mathbf{Ca}}$ and $\mathbf{i}_{\mathbf{Ca}}$ b) Current error D$\mathbf{i}_{\mathbf{Ca}}$.

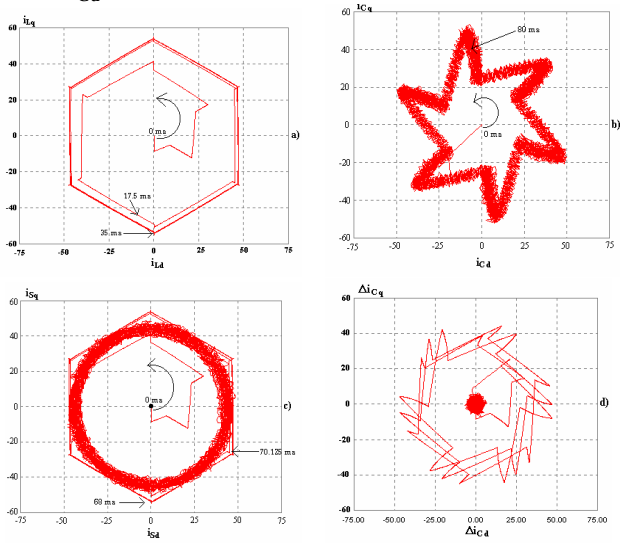

Fig. 11. Steady state space current trajectories, a) $\mathbf{i}_{\mathbf{L}}$ b) $\mathbf{i}_{\mathbf{C}}$ c) $\mathbf{i}_{\mathbf{S}}$ d) D$\mathbf{i}_{\mathbf{C}}$.

Fig. 11 shows the space current trajectories of $\mathbf{i}_{\mathbf{L}}$, $\mathbf{i}_{\mathbf{C}}$, $\mathbf{i}_{\mathbf{S}}$ and D$\mathbf{i}_{\mathbf{C}}$ before and after the active filter is switched on. Note that the $\mathbf{i}_{\mathbf{S}}$ trajectory departs from an hexagonal shape, similar to that of $\mathbf{i}_{\mathbf{L}}$, to a circular shape, when the active filter goes from the off to the on switching position. Also, the current error D$\mathbf{i}_{\mathbf{C}}$ departs from a maximum value to an almost zero value, while the compensating current $\mathbf{i}_{\mathbf{C}}$ deports from a zero value to a maximum value for the same off-on transition positions of the active filter.

Fig. 12 to 13 show conclusively an effective current vector active filter transient response at constant commutation frequency, for a sudden change of the three-phase AC/DC converter loading conditions, whose firing angle varies from 30º to 0º. In fig. 12 the quick current response of the active filter is clearly appreciated in the time oscillograms of $\mathbf{i}_{\mathbf{Sa}}$ and $\mathbf{e}_{\mathbf{a}}$ (fig. 12c). As soon as the filter switched on, $\mathbf{i}_{\mathbf{Sa}}$ become sinusoidal and in phase witch its voltage, for both $\mathbf{a}$=30º and $\mathbf{a}$=0º.

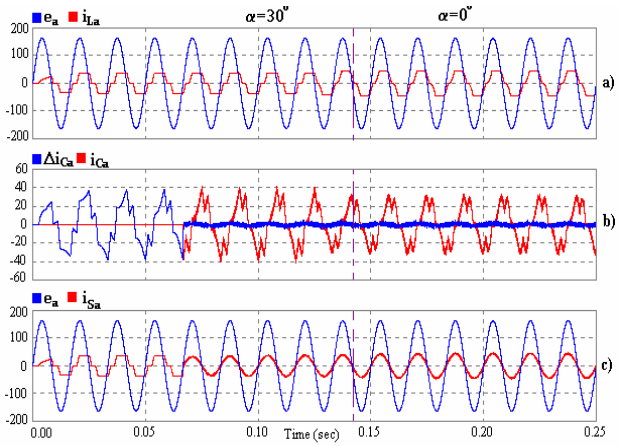

Fig. 12. Filter transient response for $\mathbf{a}$=30º and $\mathbf{a}$=0º. a) $\mathbf{e}_{\mathbf{a}}$ and $\mathbf{i}_{\mathbf{La}}$ b) D$\mathbf{i}_{\mathbf{Ca}}$ and $\mathbf{i}_{\mathbf{Ca}}$ c) $\mathbf{e}_{\mathbf{a}}$ and $\mathbf{i}_{\mathbf{Sa}}$

The space current trajectories of fig. 13 clearly exhibit their instantaneous change in trajectory, following the AC/DC transient load harmonic variations. The trajectory of $\mathbf{i}_{\mathbf{L}}$ for a load variation from $\mathbf{a}$=30º and $\mathbf{a}$=0º is shown in fig. 13a. These changes in load produces the variations in the compensating current trajectory of fig. 13b, which generates the trajectories in $\mathbf{i}_{\mathbf{S}}$ as shown in fig. 13d, which also shows the off-on transition of the active filter.

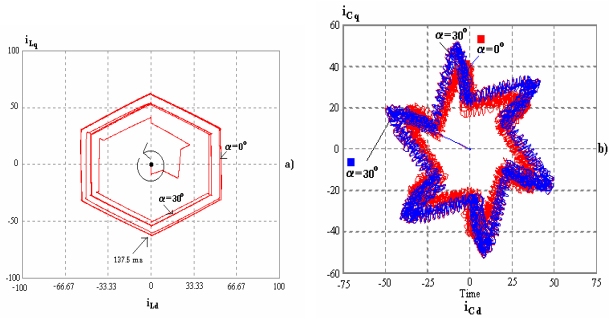

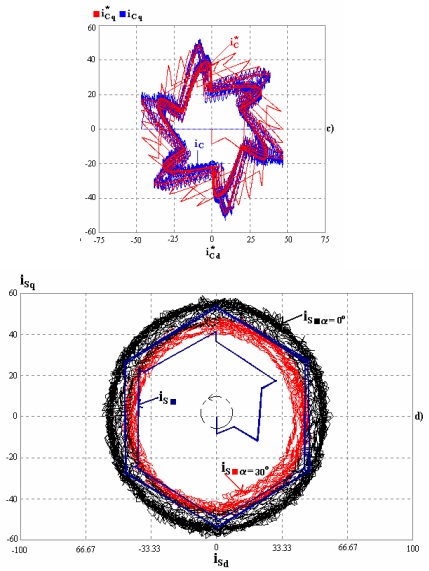

Fig. 13. Current space vector transient trajectories for **a**=30º and **a**=0º. a) $\mathbf{i_L}$ b) $\mathbf{i_C}$ c) $\mathbf{i_C^*}$ and $\mathbf{i_C}$ d) $\mathbf{i_S}$

VIII. CONCLUSIONS

- The instantaneous space trajectories of an active filter, whose compensating counterharmonic current is strictly vector controlled, has been presented.
- The vector control nature of the active filter does not require hysteresis current controllers for each one of the three compensating branches of the filter.
- The selected digital simulation results of the performance of such an active filter, have showed a quick response both for steady an transient states, to cope with the instantaneous demand of harmonic and reactive compensation.

IX. REFERENCES

[1] H. Akagi, A. Nabae and S. Atoh, "Control Strategy of Active Power Filters Using Multiple Voltaje Source PWM Converters", IEEE Trans. IAS, Vol. IA-22, No.3, pp.460, 1986.

[2] H. Akagi, Y. Kanazawa and A. Nabae, "Instantaneous Reactive Power Compensators Comprising Switching Devices Without Energy Storage Components", IEEE Trans. IAS, Vol. IA-20, pp.625, 1984.

[3] A. Nava-Segura and M. Carmona-Hernández. "A Detailed Instantaneous Harmonic and Reactive Compensation Analysis of Three-Phase AC/DC Converters, in abc and aß Coordinates". IEEE Transactions on Power Delivery, Vol. 14, No. 3, July 1999.

[4] F. Z. Peng, H. Akagi, and A. Nabae, "A Study of Active Power Filters Using Quad-Series Voltaje Source PWM Converters for Harmonic Compensation". IEEE/PESC, pp.204, 1987.

[5] A. Nabae, S. Ogasawara and H. Akagi, "A Novel Control Scheme for Current-Controlled PWM Inverters," IEEE/Trans. IAS, Vol. IA-22, No.4, pp697, 1986.

[6] H. Akagi, "Analysis and Design of an Active Power Filter Using Quad-Series Voltage-Source PWM Converters", IEEE Transactions on Industry Applications, Vol. 26, No.1 January/February 1990.

[7] D. M. Brod and D. W. Novotny, "Current control of VSI-PWM inverters," in IEEE-IAS Conf. Rec., 1984, pp. 418-425.

[8] A. Kawamura and R. G. Hoft, "Instantaneous feedback controlled PWM inverters with adaptive hysteresis," IEEE Trans. Ind. Appl., vol. IA-20, pp. 769-775, 1984.

[9] L. Malesani, P. Mattavelli, P. Tomasin, "High-Performance Hysteresis Modulation Technique for Active Filters", IEEE Trans. Power Electronics, Vol. 12. No. 5, September 1997, pp. 876-884.

[10] B. N. Singh, A. Chandra, K. Al-Haddad, "Performance Comparison of Two Current Control Techniques Applied to an Active Filter," in IEEE/PES'98 Conf. Proc., 1998, pp. 133-138.

[11] A. Nava-Segura and J. Linares-Flores. "Transient analysis of a vector controlled active filter," IEEE-IAS 2000 Conference on Industry Applications, Rome Italy, October 8- 12, 2000.